Observation of a Helical Luttinger Liquid in InAs/GaSb Quantum Spin Hall Edges

Tingxin Li, Pengjie Wang, Hailong Fu, Lingjie Du, Kate A. Schreiber, Xiaoyang Mu, Xiaoxue Liu, Gerard Sullivan, Gábor A. Csáthy, Xi Lin, and Rui-Rui Du

Phys. Rev. Lett. **115**, 136804 — Published 25 September 2015
DOI: 10.1103/PhysRevLett.115.136804

Observation of a Helical Luttinger-Liquid in InAs/GaSb Quantum Spin Hall Edges

Tingxin Li[1,4], Pengjie Wang[1,4], Hailong Fu[1,4], Lingjie Du[2], Kate A. Schreiber[3], Xiaoyang Mu[1,4], Xiaoxue Liu[1,4], Gerard Sullivan[5], Gábor A. Csáthy[3], Xi Lin[1,4], Rui-Rui Du[1,2,4]*

[1]*International Center for Quantum Materials, School of Physics, Peking University, Beijing 100871, China*

[2]*Department of Physics and Astronomy, Rice University, Houston, Texas 77251-1892, USA*

[3]*Department of Physics and Astronomy, Purdue University, West Lafayette, Indiana 47907, USA*

[4]*Collaborative Innovation Center of Quantum Matter, Beijing 100871, China*

[5]*Teledyne Scientific and Imaging, Thousand Oaks, California 91603, USA*

Abstract

We report on the observation of a helical Luttinger-liquid in the edge of InAs/GaSb quantum spin Hall insulator, which shows characteristic suppression of conductance at low temperature and low bias voltage. Moreover, the conductance shows power-law behavior as a function of temperature and bias voltage. The results underscore the strong electron-electron interaction effect in transport of InAs/GaSb edge states, which is controllable by gates. Realization of a tunable Luttinger-liquid offers a one-dimensional model system for future studies of predicted correlation effects.

It is well known that electron-electron interactions play a more important role in one-dimensional (1D) electronic system than that in higher dimensional systems. In 1D system, interactions cause electrons to behave in a strongly correlated way, so under very general circumstances, 1D electron systems can be described by Tomonaga-Luttinger liquid (LL) theory [1,2] instead of mean-field Fermi liquid theory. A Luttinger parameter K characterizes the sign and the strength of the interactions: $K < 1$ for repulsion, $K > 1$ for attraction, and $K = 1$ for non-interacting case. Confirmations of LL have been examined in various materials, such as carbon nanotubes [3-5], semiconductor nanowires [6], cleaved-edge-overgrowth 1D channel [7], as well as fractional quantum Hall (FQH) edge states [8], respectively for spinful or chiral Luttinger-liquids. The experimental hallmarks of LL are a strongly suppressed tunneling conductance and a power-law dependence of the tunneling conductance on temperature and bias voltage [3-5,8]. In a weakly disordered spinful LL, transport experiments showed that the conductance reduces from the quantized value as the temperature is being decreased [6,7].

The quantum spin Hall insulator (QSHI), also known as two-dimensional (2D) topological insulator (TI), is a topological state of matter supporting the helical edge states, which are counter-propagating, spin-momentum locked 1D modes protected by time reversal symmetry. It has recently attracted a lot of interest due to their peculiar helical edge properties and potential applications for quantum computation [9-18]. Experimentally, QSHI has been realized in HgTe quantum wells (QWs) [14] and in InAs/GaSb QWs [16-18]. In both cases, quantized conductance plateaus have been observed in devices with edge length of several micrometers [14,18], implying ballistic transport in the edges. On the other hand, devices with longer edges have lower values of conductance [14,17,18], indicating certain backscattering processes occurred inside helical edges. In principle, single-particle elastic backscattering is forbidden in helical edges due to the protection of time reversal symmetry. Therefore, inelastic and/or multiparticle scattering should be the dominating scattering mechanisms, which would lead to temperature-dependent edge conductivity [19-25]. However, in InAs/GaSb QSHI, existing experiments surprisingly show that the edge conductance is independent of temperature from 20 mK up to 30 K for both small and large samples [17,18].

The (spinless) helical LL behavior is here observed in the helical edges of InAs/GaSb QWs where the Fermi velocity of edge states is low (in the order of $v_F \sim 10^4$ m/s), resulting in strong interaction effects. Fig. 1a shows the schematic drawing of spinful LL, chiral LL, and helical LL. The dispersion of a spinful LL is linearized around the Fermi level, in comparison to the non-interaction case. The left and right moving branches of a spinful LL are always separated by a momentum of roughly $2k_F$. As for the helical LL, two branches cross at the Dirac point, thus a unique momentum-conserving umklapp scattering process [23,24] could occur near the Dirac point, in a generic (S_z symmetry broken) helical LL with sufficiently strong interactions. Also the degrees of freedom in a helical LL are only half as in a spinful LL. Fig. 1b schematically depicts the electron transport in a helical LL, where counter-propagating, strongly correlated electrons have soliton-like excitations in the ballistic transport regime.

The wafer structures for experiments are shown in Fig. 2a. Experiments are performed in two millikelvin dilution refrigerators (DR) instrumented for fractional quantum Hall effect studies, one of them having attained ~7 mK electron temperature by using a He-3 immersion cell [26], as depicted in Fig. 2b. The second DR has attained about 30 mK electron temperature [27]. The quantity, T, mentioned in the following text refer to electron temperature. Devices investigated are made with a Schottky-type front gate, showing less hysteresis effect than previous devices [17,18]. In these experiments, care is exercised to exclude spurious effects such as those from nonlinear contacts, or leaking conductance through bulk states, etc. (see section IV and VI of Supplemental Material [28]).

Fig. 2c shows the four-terminal longitudinal resistance R_{xx} as a function of the front gate voltage V_{front} in a 20×10 μm^2 six-terminal Hall bar device (wafer A) biased with different excitation currents at T~6.8 mK. R_{xx} was measured using standard low frequency (17 Hz) lock-in techniques. As the Fermi level is tuned into the QSHI gap via front gate, the R_{xx} shows a peak. Remarkably, peak values decrease with increasing current I, which indicates the helical edge has nonlinear conductance characteristics. Fluctuations can be observed in the R_{xx} peak region, and the amplitude of the fluctuations decreases with the increasing of I or T. Moreover, these fluctuations have an amplitude larger than the background noise level, and to some extent they are reproducible (see section III of Supplemental Material [28]). The inset of Fig. 2c shows the helical edge conductance $\bar{G}_{xx}$ (conductance of the averaged R_{xx} peaks) as a function of T. It can be seen that for each I value, there exists a T-independent range for $\bar{G}_{xx}$. However, the lower the current is, the narrower the T-independent range. The most likely explanation is that the helical edge conductance does not show T-dependence for the $eV >> k_BT$ regime, where k_B is the Boltzman constant. Notice that previous experiments [17,18] all used relatively high I, leading to a large eV across the helical edge, so the measured edge conductance were found to be T-independent in a large range.

We note that all devices measured here have shown these characteristic nonlinear transport. In the following we will focus on the systematic results measured from a mesoscopic two-terminal device (wafer B, edge length ~ 1.2 μm). R_{xx} was measured in a quasi-four-terminal configuration, and a series resistance ~1.9 kΩ has been subtracted for all data points. Fig. 3a shows several R_{xx}-V_{front} traces taken at different temperatures with a large bias current (500 nA). The quantized resistance plateau of $h/2e^2$ persists from 30 mK to 2 K, conforming to the behavior for $eV >> k_BT$; eventually the total conductance increases at higher T (T > 2 K) due to the delocalization of bulk states (inset in Fig. 3a). Fig. 3b shows the T-dependence of $\bar{G}_{xx}$ with two different currents from 30 mK to 1.2 K, where the bulk conductance is negligible. The measured $\bar{G}_{xx}$ with 0.1 nA excitation current can be fitted with a power-law function of T, $\bar{G}_{xx} \propto T^{\alpha}$ with exponent $\alpha \approx 0.32$. As for the I = 2 nA case, $\bar{G}_{xx}$ is independent of T in the regime where $eV >> k_BT$, then following the same power-law as the I = 0.1 nA case at higher T (T > 500 mK).

A reasonable explanation for these striking experimental observations should be based on the strong electron-electron interactions in the helical edge states of InAs/GaSb. Note that helical edge states have a topological stability that is insensitive to nonmagnetic disorder and weak interactions [11-13,19], which is in contrast with spinful LL where the conductance vanishes at T = 0 even for an arbitrarily weak disorder and interaction [2,29,30]. However, in the strong interaction regime (K< 1/4), correlated two-particle backscattering (2PB) processes are relevant [12,13,19-21] in helical edge even with a single trivial impurity (here they could be charge puddles [19,25], defects of crystalline, Rashba spin-orbit coupling [21,22], and so on), breaking the 1D helical edge into segments, thus forming a “Luttinger-liquid insulator” at T = 0. At low but finite T, $\bar{G}_{xx}$ is restored by tunneling [12,19] of excitations with fractional charge $e/2$ between energy minima inside helical edges, resulting in $\bar{G}_{xx}(T) \propto T^{2(1/4K-1)}$. A breakdown of such tunneling processes takes place when the external energy (temperature or bias voltage) is larger than the energy of the potential pinning the edge states. Therefore, the quantized conductance plateau for QSHI is recovered at large bias voltage, as we have observed.

K value of a helical LL can be estimated by formulas given in Ref. [19,31] (see section V of Supplemental Material [28]). K in HgTe QWs is about 0.8 (Ref. [31]), indicating a weak interaction regime. In InAs/GaSb QWs, K~0.22 for wafer B, is in the strong interaction regime. From the power-law exponent obtained from experiments, we deduce K~0.21, which is in good agreement with theoretical estimations.

Bias voltage dependence has also been systematically measured for the same 1.2 μm device. The inset in Fig. 4 shows the measured edge *differential* conductance dI/dV as a function of V_{dc} (the applied dc bias voltage) at various temperatures, on a double logarithmic scale. At low bias $eV_{dc} << k_BT$, dI/dV is constant with V_{dc} but the value depends on T. At higher bias, dI/dV increases with V_{dc} follows an approximate power-law, and the fitted exponent is about 0.37. Further increasing V_{dc}, dI/dV begins to deviate from the power-law behavior, tending to saturate toward the quantized value of $2e^2/h$. Furthermore, all the data points except the saturation region collapse onto a single curve if the differential conductance is scaled by T^{α} and plotted versus eV_{dc}/k_BT, as shown in Fig. 4. Similar scaling relations have been observed previously in spinful LL [3-5] and chiral LL [8], and were taken as a critical evidence of LL. Here the observed scaling relation could be suggestive for the internal tunneling processes mentioned above [12,19], since there is not any man-made tunneling barrier in our devices.

The preceding analyses are based on single impurity case, but they should still be valid for multiple, *isolated* impurities. Randomly distributed impurities may introduce a series of tunneling barriers into the helical edge, making the edge more resistive, but would not break the power-law relations. On the other hand, even without explicit impurities, uniform 2PB (umklapp) term can arise in the presence of anisotropic spin interactions [12] or just in a S_z symmetry broken helical liquid as mentioned in Ref. [23,24]. Such umklapp term in combination with strong electron-electron interaction ($K < 1/2$) leads to gap opening in the helical edge [12,32,33], or to the formation of a 1D Wigner crystal phase [34] at ultralow temperatures. When increasing the temperature or bias voltage, the umklapp processes become weakened and non-uniform so the gap becomes 'soft', resulting in a finite conductance. Future experiments such as quantum point contact [31,35] and shot-noise [19,20] measurements could in principle reveal the microscopic physical processes inside such strongly interacting helical edge states.

In conclusion, in InAs/GaSb QSHI we observe a strong suppression of the helical edge conductance at low temperature and bias voltage, which suggests that strong electron-electron interactions in the helical edges should lead to a correlated electronic insulator phase at $T = 0$ and vanishing bias voltage. Due to the fact that the bulk gaps (hence the v_F of edge states) in InAs/GaSb materials can be engineered by molecular-beam epitaxy growth and gating architectures, the electron-electron interactions can be fine-tuned, leading to a well-controlled model system for studies of 1D electronic and spin correlation physics. It's well known that [9,10] the QSHI helical edge states coupled with superconductors can support Majorana zero modes. More interestingly, the presence of strong interactions promotes these Majorana modes splitting into Z_4 parafermionic modes [32,33], which are promising for universal, decoherence-free quantum computation. The Josephson junction mediated by interacted QSHI edge states creates a pair of parafermions, yield a novel 8π-Josephson effect reflecting the tunneling processes of $e/2$ charge quasiparticles between superconductors. Further studies of interaction effects on the helical edge states in InAs/GaSb system would be necessary to advance in this direction.

We acknowledge discussions with C. L. Kane and L. I. Glazman. The work at PKU was supported by NBRPC Grant (No. 2012CB921301 and No. 2014CB920901). R.R.D. was supported by NSF Grant (No. DMR-1207562 and DMR-1508644), L.J.D. was supported by DOE Grant (No. DE-FG02-06ER46274). The ultra-low temperature transport measurements at Purdue were supported by DOE Grant (No. DE-SC0006671).

* Email: rrd@rice.edu

References

1. F. D. M. Haldane, Effective harmonic-fluid approach to low-energy properties of one dimensional quantum fluids. *Phys. Rev. Lett.* **47**, 1840-1843 (1981).
2. C. L. Kane and M. P. A. Fisher, Transport in a one-channel Luttinger liquid. *Phys. Rev. Lett.* **68**, 1220-1223 (1992).
3. M. Bockrath, D. H. Cobden, J. Lu, A. G. Rinzler, R. E. Smalley, L. Balents, and P. L. McEuen, Luttinger-liquid behaviour in carbon nanotubes. *Nature* **397**, 598-601 (1999).
4. Z. Yao, H. W. Ch. Postma, L. Balents, and C. Dekker, Carbon nanotube intramolecular junctions. *Nature* **402**, 273-276 (1999).
5. B. Gao, A. Komnik, R. Egger, D. C. Glattli, and A. Bachtold, Evidence for Luttinger-liquid behavior in crossed metallic single-wall nanotubes. *Phys. Rev. Lett.* **92**, 216804 (2004).
6. E. Levy, A. Tsukernik, M. Karpovski, A. Palevski, B. Dwir, E. Pelucchi, A. Rudra, E. Kapon, and Y. Oreg, Luttinger-liquid behavior in weakly disordered quantum wires. *Phys. Rev. Lett.* **97**, 196802 (2006).
7. A. Yacoby, H. L. Stormer, Ned S. Wingreen, L. N. Pfeiffer, K. W. Baldwin, and K. W. West, Nonuniversal conductance quantization in quantum wires. *Phys. Rev. Lett.* **77**, 4612-4615 (1996).
8. A. M. Chang, L. N. Pfeiffer, and K. W. West, Observation of chiral Luttinger behavior in electron tunneling into fractional quantum Hall edges. *Phys. Rev. Lett.* **77**, 2538-2541 (1996).
9. M. Z. Hasan and C. L. Kane, Colloquium: Topological insulators. *Rev. Mod. Phys.* **82**, 3045-3067 (2010).
10. X. L. Qi and S. C. Zhang, Topological insulators and superconductors. *Rev. Mod. Phys.* **83**, 1057-1110 (2011).
11. C. L. Kane and E. J. Mele, Z_2 topological order and the quantum spin Hall effect. *Phys. Rev. Lett.* **95**, 146802 (2005).
12. C. J. Wu, B. A. Bernevig, and S. C. Zhang, Helical liquid and the edge of quantum spin Hall systems. *Phys. Rev. Lett.* **96**, 106401 (2006).

13. C. Xu and J. E. Moore, Stability of the quantum spin Hall effect: Effects of interactions, disorder, and Z_2 topology. *Phys. Rev. B* **73**, 045322 (2006).

14. M. König, S. Wiedmann, C. Brüne, A. Roth, H. Buhmann, L. W. Molenkamp, X. L. Qi, and S. C. Zhang, Quantum spin Hall insulator state in HgTe quantum wells. *Science* **318**, 766-770 (2007).

15. C. X. Liu, T. L. Hughes, X. L. Qi, K. Wang, and S. C. Zhang, Quantum spin Hall effect in inverted type-II semiconductors. *Phys. Rev. Lett.* **100**, 236601 (2008).

16. I. Knez, R. R. Du, and G. Sullivan, Evidence for helical edge modes in inverted InAs/GaSb quantum wells. *Phys. Rev. Lett.* **107**, 136603 (2011).

17. E. M. Spanton, K. C. Nowack, L. J. Du, G. Sullivan, R. R. Du, and K. A. Moler, Images of edge current in InAs/GaSb quantum wells. *Phys. Rev. Lett.* **113**, 026804 (2014).

18. L. J. Du, I. Knez, G. Sullivan, and R. R. Du, Robust helical edge transport in gated InAs/GaSb bilayers. *Phys. Rev. Lett.* **114**, 096802 (2015).

19. J. Maciejko, C. X. Liu, Y. Oreg, X. L. Qi, C. J. Wu, and S. C. Zhang, Kondo effect in the helical edge liquid of the quantum spin Hall state. *Phys. Rev. Lett.* **102**, 256803 (2009).

20. N. Lezmy, Y. Oreg, and M. Berkooz, Single and multiparticle scattering in helical liquid with an impurity. *Phys. Rev. B* **85**, 235304 (2012).

21. F. Crépin, J. C. Budich, F. Dolcini, P. Recher, and B. Trauzettel, Renormalization group approach for the scattering off a single Rashba impurity in a helical liquid. *Phys. Rev. B* **86**, 121106(R) (2012).

22. F. Geissler, F. Crépin, and B. Trauzettel, Random Rashba spin-orbit coupling at the quantum spin Hall edge. *Phys. Rev. B* **89**, 235136 (2014).

23. T. L. Schmidt, S. Rachel, F. von Oppen, and L. I. Glazman, Inelastic electron backscattering in a generic helical edge channel. *Phys. Rev. Lett.* **108**, 156402 (2012).

24. N. Kainaris, I. V. Gornyi, S. T. Carr, and A. D. Mirlin, Conductivity of a generic helical liquid. *Phys. Rev. B* **90**, 075118 (2014).

25. J. I. Väyrynen, M. Goldstein, Y. Gefen, and L. I. Glazman, Resistance of helical edges formed in a semiconductor heterostructure. *Phys. Rev. B* **90**, 115309 (2014).

26. N. Samkharadze, A. Kumar, M. J. Manfra, L. N. Pfeiffer, K. W. West, and G. A. Csáthy

Integrated electronic transport and thermometry at milliKelvin temperatures and in strong magnetic fields. *Rev. Sci. Instrum.* **82**, 053902 (2011).

27. X. B. Wang, H. L. Fu, L. J. Du, X. X. Liu, P. J. Wang, L. N. Pfeiffer, K. W. West, R. R. Du, and X. Lin, Depinning transition of bubble phases in a high Landau level. *Phys. Rev. B* **91**, 115301 (2015).
28. See Supplemental Material for methods, gate hysteresis, transport measurements of Corbino devices, estimation of *K* values, and contact issues.
29. D. L. Maslov, Transport through dirty Luttinger liquids connected to reservoirs. *Phys. Rev. B* **52**, R14368-R14371 (1995).
30. A. Furusaki and N. Nagaosa, Kondo effect in a Tomonaga-Luttinger liquid. *Phys. Rev. Lett.* **72**, 892-895 (1994).
31. J. C. Y. Teo and C. L. Kane, Critical behavior of a point contact in a quantum spin Hall insulator. *Phys. Rev. B* **79**, 235321 (2009).
32. F. Zhang and C. L. Kane, Time-Reversal-Invariant Z_4 Fractional Josephson Effect. *Phys. Rev. Lett.* **113**, 036401 (2014).
33. C. P. Orth, R. P. Tiwari, T. Meng, and T. L. Schmidt, Non-Abelian parafermions in time-reversal-invariant interacting helical systems. *Phys. Rev. B* **91**, 081406(R) (2015).
34. N. T. Ziani, F. Crépin, and B. Trauzettel, Fractional Wigner crystal in the helical Luttinger liquid. arXiv:1504.07143v1 (2015).
35. C. Y. Hou, E. A. Kim, and C. Chamon, Corner junction as a probe of helical edge states. *Phys. Rev. Lett.* **102**, 076602 (2009).

Figure Captions

FIG. 1 Family of Luttinger-liquids. (a) Schematic drawing of energy dispersions for spinful LL, chiral LL, and helical LL, respectively; for the spinful LL, two straight lines illustrate the linearized dispersion, corresponding to the left and right moving branches, respectively. In the chiral LL, strongly correlated, spin degenerated electrons move in only one direction. As for the helical LL, the left and right moving branches cross at the Dirac point, and electrons with opposite spins move in opposite directions. (b) Schematic drawing of the electron transport in a helical LL.

FIG. 2 (a) Specific structures of two InAs/GaSb wafers used for experiments. (b) Schematic drawing of the He-3 immersion cell [26]. Orange, light grey, dark grey and black parts represent copper, polycarbonate, silver, and the sample, respectively. The cell is attached to the mixing chamber of the DR and filled with liquid He-3 through a capillary. Contacts of the sample are soldered with indium to several heatsinks which are made of 100-500 nm silver powder sintered on to silver wires. (c) R_{xx} of a 20×10 μm^2 Hall bar made by wafer A versus V_{front} at T~6.8 mK biased with different currents. Inset in **c**, helical edge conductance $\bar{G}_{xx}$ as a function of T. At 0.1 nA, $\bar{G}_{xx}$ begins to change for $T > 60$ mK, and the critical T is about 160 mK for the 1 nA case. As for the 10 nA case, there is no obvious change of $\bar{G}_{xx}$ below 250 mK.

FIG 3. Temperature dependence for a mesoscopic device (wafer B, edge length ~1.2 μm). (a) R_{xx}–V_{front} traces taken at 30 mK, 350 mK, 1 K, and 2 K with 500 nA excitation current. Quantized resistance plateau of $h/2e^2$ persists from 30 mK to 2 K. Inset in (a), plateau conductance increases at higher temperature due to delocalized bulk carriers. (b) Temperature dependence of the helical edge conductance $\bar{G}_{xx}$ with I = 0.1 nA, and 2 nA. The straight line on the log-log plot indicates a power-law behavior $\bar{G}_{xx} \propto T^{0.32}$. Inset in (b) shows the SEM image of the device.

FIG 4. Bias voltage dependence for a mesoscopic device (wafer B, edge length ~1.2 μm). The inset shows V_{dc} dependence of the edge differential conductance dI/dV measured at T = 50 mK, 100 mK, 350 mK, and 1 K, with the ac modulation current I_{ac} = 0.1 nA. The solid line indicates a power-law of $dI/dV \propto V_{dc}^{0.37}$. The main plot illustrates all the measured data points except the saturation region collapse onto a single curve by scaling the measured d*I*/d*V*.

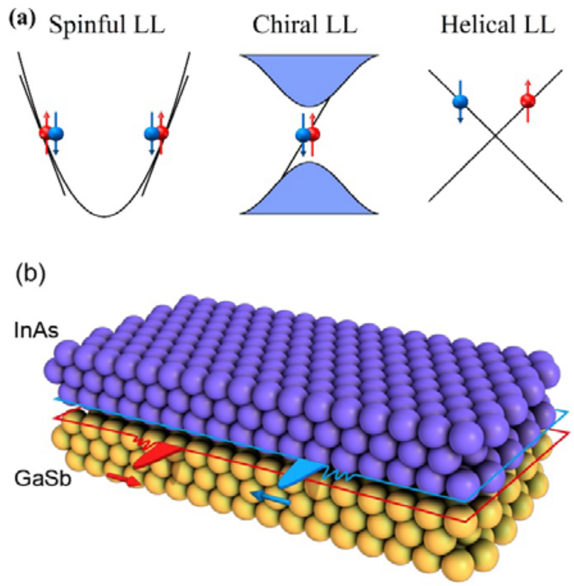

Figure 1

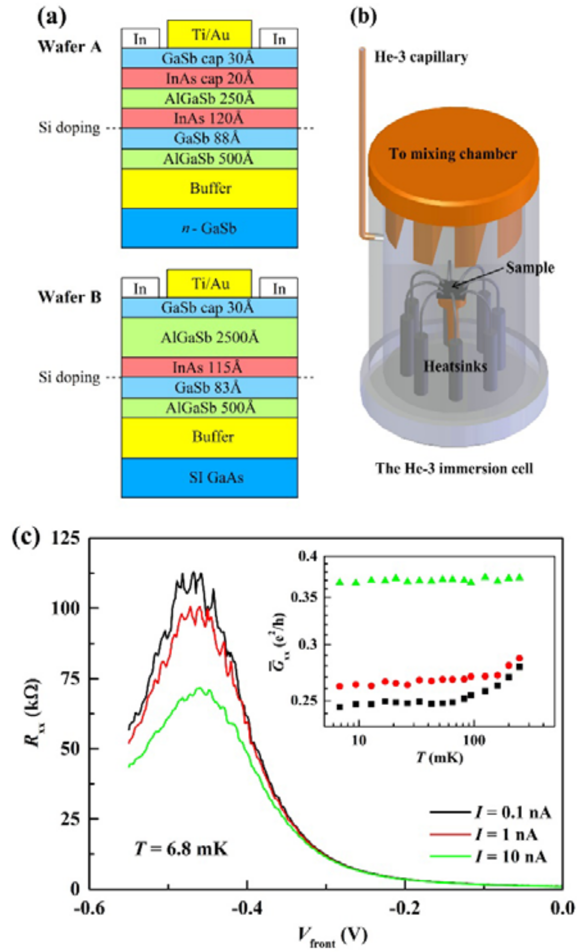
(a)
Wafer A
In
Ti/Au
In
GaSb cap 30Å
InAs cap 20Å
AlGaSb 250Å
Si doping
InAs 120Å
GaSb 88Å
AlGaSb 500Å
Buffer
n - GaSb
Wafer B
In
Ti/Au
In
GaSb cap 30Å
AlGaSb 2500Å
Si doping
InAs 115Å
GaSb 83Å
AlGaSb 500Å
Buffer
SI GaAs
(b)
He-3 capillary
To mixing chamber
Sample
Heatsinks
The He-3 immersion cell
(c)
T = 6.8 mK
I = 0.1 nA
I = 1 nA
I = 10 nA
V_front (V)
R_xx (kΩ)
T (mK)

Figure 2

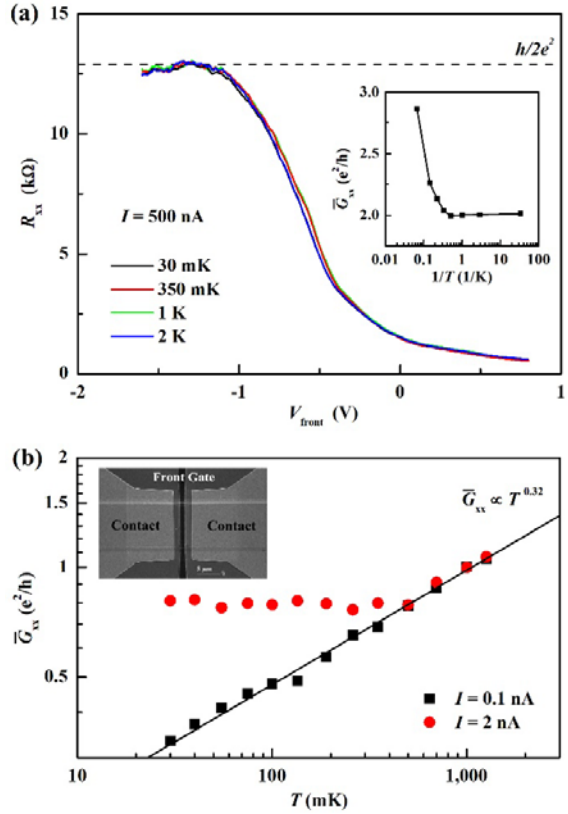
(a)
h/2e²
I = 500 nA
30 mK
350 mK
1 K
2 K
R_xx (kΩ)
V_front (V)
Ḡ_xx (e²/h)
1/T (1/K)
(b)
Front Gate
Contact
Contact
Ḡ_xx ∝ T^0.32
I = 0.1 nA
I = 2 nA
Ḡ_xx (e²/h)
T (mK)

Figure 3

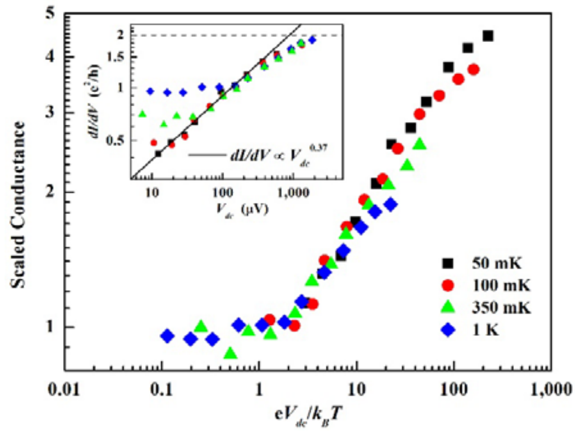
Scaled Conductance
5
4
3
2
1
0.01
0.1
1
10
100
1,000
eV_{dc}/k_BT
50 mK
100 mK
350 mK
1 K
dI/dV (e^2/h)
2
1.5
1
0.5
10
100
1,000
V_{dc} (μV)
$dI/dV \propto V_{dc}^{0.37}$

Figure 4